Post DC Fault Circulating Current Suppression Control

Tarcar, Rohan Kamat; Shetgaonkar, Ajay; Popov, Marjan; Van Der Meijden, Mart; Winter, Wilhelm; Ndreko, Mario; Dimitrovski, Robert; Burkhardt, Matthias; Lekić, Aleksandra

DOI
10.1109/PESGM52003.2023.10252199

Publication date
2023

Document Version
Final published version

Published in
2023 IEEE Power and Energy Society General Meeting, PESGM 2023

Post DC Fault Circulating Current Suppression Control

Rohan Kamat Tarcar, Ajay Shetgaonkar (*Student Member, IEEE*), Marjan Popov (*Fellow, IEEE*), Mart van der Meijden, Wilhelm Winter, Mario Ndreko, Robert Dimitrovski, Matthias Burkhardt, and Aleksandra Lekić (*Senior Member, IEEE*)

2023 IEEE Power & Energy Society General Meeting (PESGM) | 978-1-6654-6441-3/23/$31.00 ©2023 IEEE | DOI: 10.1109/PESGM52003.2023.10252199

***Abstract*—The radial topology of the Multi-terminal High Voltage Direct Current (MTDC) power system is a preferred connection for the gigawatt- renewable power due to its scalability and reliability. However, a radial topology with a metallic return bipolar converter configuration MTDC network possesses technical challenges regarding DC fault current interruption and grid expansion. Furthermore, such HVDC networks are energized in a specific manner, usually involving a separate energizing controller. This paper proposes a design of DC Hubs with direct current circuit breakers (DCCBs) along with a network energization sequence without requiring a separate controller. Additionally, a PI-based controller for post-DC fault circulating current in MTDC's metallic return is proposed. This control operates after DCCB recloses, removing any offset in the metallic cable by regulating the power setpoint in the converters. The proposed control is investigated under a pole-to-ground fault occurrence in the DC Hub. The proposed solution is validated by RSCAD/RTDS® simulation by applying detailed and average equivalent models of turbines, DCCBs and converters. The results of this simulation show a successful suppression of the DC circulating current, which results in a balanced operation of the MMCs in the post fault steady state conditions.**

***Index Terms*—MTDC, Bipolar MMC, Metallic return, Startup Sequence, Current Suppression Control, RTDS, VARC DCCB**

I. Introduction

Modular multilevel converter (MMC) based transmission is preferred for large offshore renewable power generation due to its scalability, controllability and reliability [1]. In recent years, numerous point-to-point (P2P) MMC-based high-power direct current (HVDC) transmission links are either built or planned in Europe. The P2P topology is the simplest HVDC network, but one of the major disadvantages is that adding new terminals to the existing network is not possible without building a new network [2]. To meet European Union (EU) goals, Mesh Offshore Grid (MOG) is a proposed concept in European research projects [3].

Among different MOG topologies, the radial topology is selected because of its improved onshore grid reliability and resiliency [4], along with the better utilization of generation and transmission infrastructures [5]. A bipolar metallic return configuration is proposed for the terminal implementations of this radial topology due to $N-1$ contingency. Furthermore, an offshore Hub is planned at the Bornholm island, CleanStream energy Hub, which would increase system reliability. The design of the offshore Hub is challenging due to its large footprint and costs [6]. Thus, the onshore DC Hub is proposed instead. DC Hub comprises a DC bus bar and a direct current circuit breaker (DCCB). The DCCB protects the MTDC against DC faults by interrupting the faulty interconnection. Over decades of research on DCCB, different DCCB topologies have been proposed. Voltage source converter assisted resonant current (VARC) DCCB is selected in this study due to its fast fault interruption capabilities, low conduction loss, and cost-effectiveness. [7]–[10]. However, the energization of the radial grid with DCCBs is not sufficiently explored. Therefore, this paper proposes a missing solution for the energization and post-fault circulating current suppression.

The start-up sequence proposed in [11], requires a separate control to ensure a safe energization of the networks as the network does not contain DCCBs. The sequence described in [12] involves the insertion of resistors with associated bypass breakers. Implementing the DC-Hub and DCCBs makes it possible to realize an energization sequence without needing a separate black start control. This start-up sequence is addressed in this paper. Furthermore, these start-up sequences apply only to specific scenarios with rigid bipoles or only monopolar configuration of the MMCs in the network or with LCC rather than VSC in the converter stations, in which the zero current or zero voltage modes of start up are used, the latter being in which the DC voltage is initially limited to 0.5 pu till the converter reaches its rated value and, vice versa [13].

Another contribution of this paper is the circulating current suppression on the DC side of the bipolar MMC-based power system after a DC fault interruption. The circulating current in MMCs is usually controlled inside the MMCs by applying a circulating current suppression control (CCSC) [14]–[16]. A few more current suppression controllers that use proportional resonant control only work well when the number of submodules is high [17], [18], contrary to the controller discussed in this paper, which is not dependent on the number of submodules. Upon DC fault current interruption in a bipolar metallic configuration, the nominal current flows through the metallic return. Furthermore, after the re-close of the DCCB, a circulating current leaks into the metallic return path of the cable. As a result, there is a power imbalance in the network during the post-fault period. To our knowledge, evidence has yet to be reported in the literature explaining the mentioned phenomena. Hence, the circulating current is generally left uncontrolled [19]. In this paper, the aforementioned circulating current on the DC side is referred to as the residual metallic return current.

This paper discusses a new energization/startup sequence

R. K. Tarcar, A. Shetgaonkar, M. Popov, and A. Lekić are with the Faculty of Electrical Engineering, Mathematics and Computer Science, Delft University of Technology, Delft, The Netherlands (correspondence e-mails: {M.Popov, A.Lekic}@tudelft.nl)

M. vd Meijden is with TenneT TSO B.V., Arhnem, The Netherlands(e-mail: Mart.vander.Meijden@tennet.eu)

W. Winter, M. Ndreko, R. Dimitrovski and M. Burkhardt are with TenneT GmbH, Bayreuth, Germany (e-mails: {Wilhelm.Winter, Mario.Ndreko, Robert.Dimitrovski, Matthiassebastian.Burkhardt}@tennet.eu).

978-1-6654-6441-3/23/$31.00 ©2023 IEEE

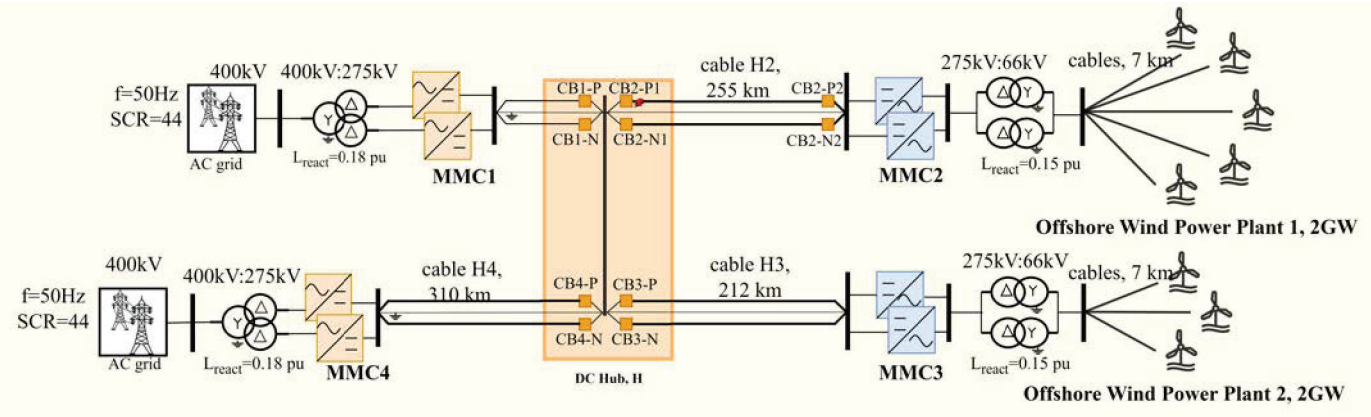

Fig. 1: A four-terminal ± 525 kV bipolar half-bridge MMC-based HVDC system with a metallic return, and a DC Hub.

and a DC circulating current suppression controller for the dedicated metallic return. Furthermore, the implementation of a DC Hub and VARC DCCBs makes the use of an energization sequence without a separate startup controller possible, and they are tested for a pole-to-ground (PG) fault condition on a Real Time Digital Simulator (RTDS$^{@}$). Both the startup sequence and the suppression controller can be easily implemented in bipolar MMC-based HVDC networks with DCCBs, which are installed for the system's protection.

Section II deals with the description of the MTDC network/model. The starting sequence of the network is stated in Section III. The effect of the post-fault circulating current and the mitigation effect of the zero current controller is presented in Section IV. The results are presented and discussed in Section V, and finally, the paper ends with meaningful conclusions presented in Section VI.

II. Network Description

The studied system is an offshore ± 525 kV bipolar metallic return four-terminal HVDC network with a DC Hub, as shown in Fig.1. The network studied in Cigre B4.72 was taken as a basis for the development of the studied system [19]. It consists of two onshore stations, an onshore DC Hub, and two offshore stations. The onshore stations are connected to the AC grid, whereas the offshore converter stations are connected to the wind power plants (WPPs). The topology of this network is a radial, with the Hub being the central node. All MMCs (i.e. converter stations) makes use of half-bridge submodules with a bipolar connection. The MMCs denoted as MMC4, the negative pole of MMC1 and the negative pole of MMC2 are modelled as average value models in RSCAD/RTDS (known as type 5). All other MMCs in the network are modelled as GTFPGA-based detailed equivalent RSCAD/RTDS models (known as type 2) [20]. The onshore stations are connected to the Thevenin's equivalent circuit of a strong grid ($SCR = 44$), and the offshore stations are connected to the average value-based wind turbines.

The DC Hub (switchyard) enables installation of VSC-assisted resonant current direct current circuit-breakers (VARC DCCBs) on the cables connecting the Hub to the converter stations. The cable connecting the DC Hub with MMC2 (cable H2) is 255 km long, the cable from the Hub to MMC3 (cable H3) is 212 km long, and the cable joining the Hub with MMC4 (cable H4) is 310 km long. MMC1 is directly connected to the Hub through the DCCBs. The cables are modelled as frequency dependent (phase) model. Furthermore, due to metallic return topology, the cable link consists of 3 cables (i.e., a positive, a negative, and a metallic return cable in one cable connection). The network topology is designed in such a way to have one set of VARC DCCBs on cable H3. There are no DCCBs at the offshore end of the cables due to technical and economic factors. To investigate the impact of offshore DCCB on the network during pre and post-transient disturbance, we placed a DCCB at the end of cable H3 (the end that is far away from the MMC).

The offshore converters are connected to the WPPs by 7 km AC cables. The plant that is connected to MMC2 uses 5 wind turbines, and the other one connected to MMC3 has 3 wind turbines. The onshore capacity of each converter station is 6 GW, whereas that of offshore is 4 GW. The capacity of the wind turbine is 5 MW. However, the total capacity of each WPP is scaled to 2 GW using a scaling transformer to have WPPs with practical capacities. Table I shows additional network specifications. The network is designed to have $N-1$ security as each MMC in the offshore converter station is designed to handle 2 GW of power, ensuring full power flow even during faults in one of the cables connected to the MMCs. The control strategies implemented for each converter stations are listed in Table II.

It should be noted that following assumptions are made during the modelling:

- When the positive pole of MMC is mentioned, it refers to the upper MMC of the bipolar MMC configuration connected to the positive pole of the cable. Similarly, the negative pole of the MMC refers to the lower MMC of the same bipolar configuration, connected to the negative pole of the DC cable.
- When the power is consumed, the sign of active power (P) and reactive power (Q) is positive (*+ve*), and if the power is generated the sign if active power (P) and reactive power (Q) is negative (*-ve*).
- During the startup sequence, the protection protocols in place are temporarily disabled to avoid the spikes in the active power during pole closure. This is caused by the DC control strategy of MMC1.

III. Starting Sequence

The energization of the MTDC requires a startup sequence to ensure that the system will operate nominally [21]. This

978-1-6654-6441-3/23/$31.00 ©2023 IEEE

TABLE I: Network specifications

Parameter	Onshore	Offshore
Transformer capacity	6 GW	4 GW
Rated grid line-line voltage	400 kV	66 kV
Transformer voltage ratio	400/275 kV	275/66 kV
Transformer leakage reactance	0.18 pu	0.15 pu
Transformer configuration	Yn-D, 1P3W	D-Yn, 3P2W
DC line inductances	80 mH	80 mH
No. of MMC Submodules	240	240
Submodule capacitance	25 mF	16 mF
Converter Inductance	50 mH	50 mH

TABLE II: Control strategy specifications of the converters in the network

Converter	Control mode	Added Description
MMC1	V_{dc}, V_{ac}	$V_{dc,ref} = 525$ kV, $V_{ac,ref} = 400$ kV
MMC2	V_{ac}, f	$V_{ac,ref} = 66$ kV, $f_{ref} = 50$ Hz
MMC3	V_{ac}, f	$V_{ac,ref} = 66$ kV, $f_{ref} = 50$ Hz
MMC4	P, Q	$P_{ref} = 2000$ MW, $Q_{ref} = 0$ MW

sequence is also crucial for the precharging of the MMCs' submodule capacitors [11]. The proposed startup sequence considers the control strategies implemented for the network converter stations and the control strategies' settling times. The sequence proposed is as follows:

- Deblocking of the MMCs in MMC1 and closure of the VARC DCCBs (CB1-P and CB1-N) occurs simultaneously, thereby the DC voltage to ± 525 kV on the terminals. MMC1 sets the reference voltage for the DC Hub and then the Hub charges all the cables.
- Deblocking of the MMCs in MMC2 and closing VARC DCCBs (CB2-P1,2 and CB2-N1,2) is only done after the terminal DC voltage is stabilized at ± 525 kV. This ensures a stable rise in the voltage of MMC2 with minimal disturbances. WPP 1 is then started and deblocked to increase the terminal voltage of MMC2 to 530 kV.
- The energization of MMC3 is the same as that of MMC2, as the control strategy and the power capacities of the MMCs, as well as the WPP connected, are the same.
- Since the MMCs in the MMC4 are controlled in *P,Q* control strategy, the active power of the MMCs is set to consume 2 GW. Therefore, this converter is deblocked, and the VARC DCCBs (CB4-P and CB4-N) are closed, only after the total production of active power is more than 2 GW. Hence, MMC4 is deblocked after the total production is 4 GW. This ensures that MMC4 gets 2 GW of active power, so that the controls can operate as expected.

Table III also lists the events that occur during the startup sequence in chronological order.

Fig. 2 shows the variation of the DC voltage and the active power during the start-up sequence of the network. Since the rated DC voltage of the network is ± 525 kV, the measured DC pole-to-pole voltage is 1050 kV which is used for the per-unit conversion of the DC voltages. Furthermore, according to the CIGRE and ENTSO-E standards, the over- and under-shoot of the voltages should be within the $\pm 10\%$ margin [22], which can be seen as valid in Fig.2. Since the onshore converters (MMC1 and MMC4) are connected to the onshore strong AC grid, the total blocking voltage of the MMCs in the rectifier

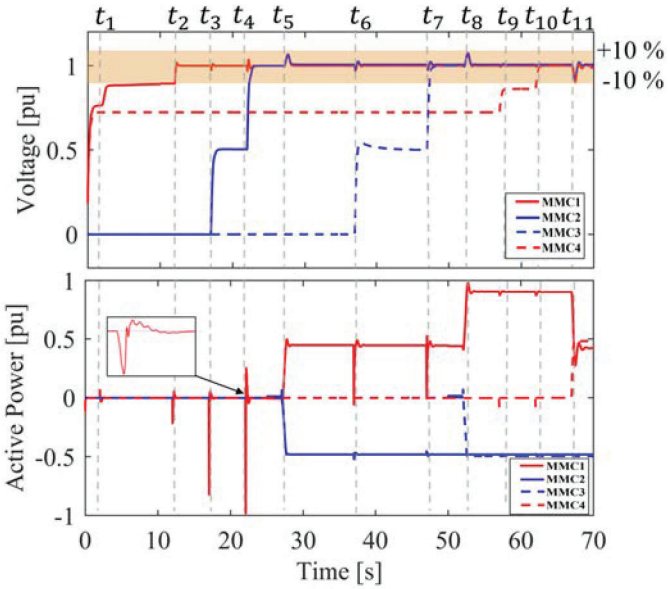

Fig. 2: Behavior of DC voltages and active power during the system's startup.

TABLE III: Sequence of events with their time instants during the startup

Time-step	Events
$\mathbf{t_1}$	MMC1 positive pole is deblocked and CB1-P is closed
$\mathbf{t_2}$	MMC1 negative pole is deblocked and CB1-N is closed
$\mathbf{t_3}$	MMC2 positive pole is deblocked; CB2-P1 and CB2-P2 is closed
$\mathbf{t_4}$	MMC2 negative pole is deblocked; CB2-N1 and CB2-N2 is closed
$\mathbf{t_5}$	Offshore WPP 1 is started and deblocked
$\mathbf{t_6}$	MMC3 positive pole is deblocked and CB3-P is closed
$\mathbf{t_7}$	MMC3 negative pole is deblocked and CB3-N is closed
$\mathbf{t_8}$	Offshore WPP 2 is started and deblocked
$\mathbf{t_9}$	CB4-P is closed
$\mathbf{t_{10}}$	CB4-N is closed
$\mathbf{t_{11}}$	MMC4 is deblocked

mode is about $0.6pu$ (this is before the DCCBs of the onshore converters are closed and the converters are deblocked). This starting sequence also considers the voltage surges that occur when the VARC DCCBs are closed. Therefore, the breakers on the positive pole are closed first, and only after the positive pole voltage has reached its specified value of $+525$ kV, the DCCB on the negative pole is closed.

Additionally, the spikes observed in the active power curve of MMC1 from Fig. 2 are caused by the sudden voltage fluctuation when DCCBs close. Namely, the DC voltage control of MMC1 tries to reach its set point, which causes an unconventional spike in the active power at those time instances. The voltage and active power spikes are observed to be in proportion to the distance of the DC cable, i.e. the longer the cable, the bigger the fluctuation spikes. The final dip of the voltages and the active power at t_{11} is caused by deblocking of the MMC4, which is governed by *P,Q* control.

This unique sequence is only possible because of the presence of VARC DCCBs in the DC Hub, which allows rapid connection and disconnection of the cables in the network.

978-1-6654-6441-3/23/$31.00 ©2023 IEEE

IV. Post fault DC circulating current suppression control

A. Post fault DC circulating current imbalance

The metallic ground return implemented with the bipolar configuration of the MMCs, provides a return path for the current during and after fault current interruption. A temporary PG fault was implemented on the positive pole of the cable H2, at the point of contact between the DC Hub, and the positive pole cable termination. This fault, in reality, could resemble a faulty contact and therefore have real-life inferences. Since this fault is between the DC Hub and MMC2, some major observations were made in MMC2. It was observed that the rapid de-energization and energization of the MMC during and after the fault, and the closure of the DCCB pole led to a residual current in the metallic return. This residual circulating DC current causes an imbalance in the DC currents in the poles of the cables. This imbalance further created a magnitude difference in the DC voltages, and the active and reactive powers of the MMC2 and the power transferred through the cable H2, as seen in Table IV. The metallic return current is also depicted in Fig. 4.

Fig. 4 shows the current through the dedicated metallic return of cable H2. Before the fault is imposed, the current through the metallic return is observed to be 0 kA, which is in line with the nominal operating conditions. At the time instance t_f, the PG fault is imposed and the transient current rushes through the metallic return. After the fault has cleared, the current through the metallic return is around 3 kA, which is according to the expectation since only one pole (negative) is still in operation. All of the planned 2 GW of power flows through this pole. At t_c, when the CB2-P1 and CB2-P2 are closed, another spike in the metallic return current is observed before reaching a steady state value of 0.32 kA. This residual current is responsible for the imbalance caused in the MMC bipolar converters, the power delivered through cable H2, and the currents in cable H2, as seen in Table IV.

B. DC circulating current suppression control

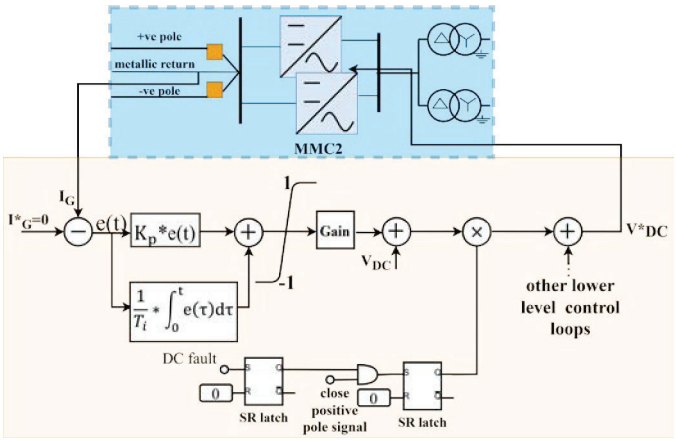

Fig. 3: Block diagram of the zero-current controller.

As a solution for the post-fault metallic return current imbalance, a PI controller was implemented and tuned to counteract the imbalance observed in Fig. 4. Fig. 3, shows the block diagram of the controller. The current from the metallic return is fed into the PI control loop, and the output of this loop is fed to V_{dc}^*, i.e. lower-level control of the MMC. The current from the metallic return is compared against the metallic return reference current I_G^*, which is set to be $0pu$. This facilitated the suppression of metallic return current, resulting in the positive and negative pole DC currents to be nearly equal in magnitude, thereby balancing all the parameters of the bipolar MMC station. The controller is only activated after the fault has been cleared and the DCCBs have been closed after the fault clearance event, as there is no necessity for this controller during the start-up sequence or during the occurrence of a fault. This controller's function is to suppress the residual metallic return current in the cable after the fault. The activation logic is depicted in Fig. 3. For the controller, the integral gain $T_i = 5$ s makes it a slow-type controller, and its proportional gain is $K_p = 1$. The controller is not deactivated as it does not affect the normal operation of the network.

V. Verification of the proposed control

As seen in Fig. 4, the controller is added to suppress the residual current in the metallic return. It can be seen that up until time instance $t = t_c$, the current signal with the controller retraces the path of the current without the controller. But, after $t = t_c$, the metallic return current with the controller, is having a steeper slope, and reaches a lower value of current faster than the one without the controller. The zoomed portion of Fig. 4 shows that the second peak of the controlled current (9 A) is much lower than the uncontrolled current (1.2 kA) at the same time instant $t = 13.2$ s. The steady-state amplitude of the metallic return current is found to be 7 A, while the magnitude of the metallic return current without the controller was 320 A. From Fig. 5 and Table IV, it is also observed that

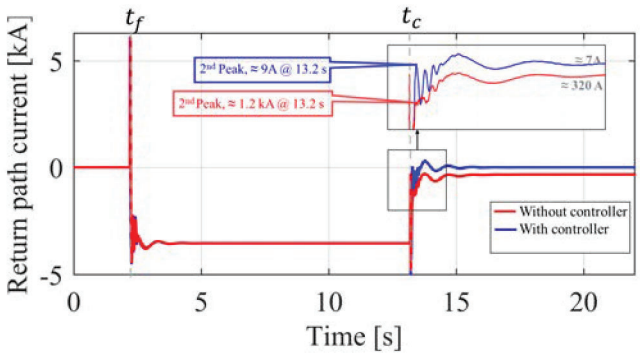

Fig. 4: Metallic return current behaviour with and without the controller.

with the addition of the current suppression controller, the MMC2 operates in the steady-state. Therefore, the imbalance caused in the DC currents of cable H2 previously is removed. Furthermore, this controller was tested for a positive and negative PG fault for different locations on cable H2. Likewise, the investigation was extended for a capacitive, inductive, and resistive DC fault. Under these scenarios, the controller suppresses the return path current as it does in the case of a positive PG fault. Therefore, the return path current plots for these scenarios are similar to Fig. 4.

978-1-6654-6441-3/23/$31.00 ©2023 IEEE

TABLE IV: Comparison of MMC2's parameters without and with the controller

MMC2	Without controller			With controller		
	Positive pole	Negative pole	Metallic return	Positive pole	Negative pole	Metallic return
DC currents (kA)	1.645	-1.964	**-0.3187**	1.821	-1.814	**- 0.00705**
Power transferred (MW)	871.2	1043	172	960.3	955	5.1
Active Power of MMC (MW)	-1002	-1050	-	-964.4	-960.4	-
Reactive Power of MMC (Mvar)	104.8	-496.8	-	-58.87	-57.74	-
DC voltage (kV)	528.8	-529.5	-	529.1	529.1	-

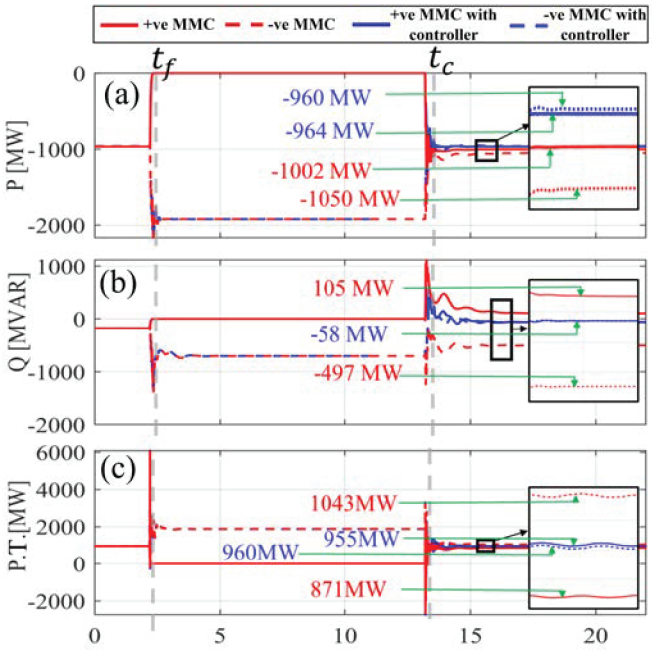

Fig. 5: MMC2 parameters with and without the controller: (a) MMC2 active power, (b) MMC2 reactive power, and (c) power transferred through cable H2.

VI. Conclusion

The paper deals with the development of the startup sequence of the radial MMC-based HVDC network with a metallic return. This sequence is centered around the control strategies implemented for the converters, and the settling times of these strategies rather than devising a separate control for the network energization. This startup sequence is credited to the presence of a DC Hub and the implementation of VARC DCCBs. The paper highlights the mitigation of the DC circulating current observed due to the bipolar configuration. It is established by the controller used for the suppression of the DC circulating current and thereby making the DC currents in the cable equal in magnitude. This controller is a PI controller, that is easy to implement, and provides a viable solution whenever such imbalances in bipolar MMC-based HVDC converters take place. The only trade-off realized during the controller implementations is that the controller can only operate after the fault has been cleared and the circuit breakers are closed. In this work, the current suppression controller is not deactivated as mentioned in IV-B. Therefore, future work will address the deactivation strategy of the current suppression controller.

References

[1] F. Martinez-Rodrigo, S. de Pablo, and L. C. Herrero-de Lucas, "Current Control of a Modular Multilevel Converter for HVDC Applications," *Renewable Energy*, vol. 83, pp. 318–331, 2015.

[2] A. Raza, A. Mustafa, U. Alqasemi, K. Rouzbehi, R. Muzzammel, S. Guobing, and G. Abbas, "HVDC Circuit Breakers: Prospects and Challenges," *Applied Sciences*, vol. 11, no. 11, p. 5047, 2021.

[3] "PROMOTiON D7.4 Economic Framework for a Meshed Offshore Grid," Brochure, 2019. [Online]. Available: https://www.promotion-offshore.net/results/deliverables/

[4] J. P. Pfeifenberger, J. Tsoukalis, and S. A. Newell, "The Benefit and Cost of Preserving the Option to Create a Meshed Offshore Grid for New York," 2021.

[5] T. M. Haileselassie and K. Uhlen, "Power System Security in a Meshed North Sea HVDC Grid," *Proceedings of the IEEE*, vol. 101, no. 4, pp. 978–990, 2013.

[6] J. N. M. Task-12.3, Task lead-TenneT TSO B.V., "PROMOTiON d12.4 Final Deployment Plan," Brochure, 2020. [Online]. Available: https://www.promotion-offshore.net/results/deliverables/

[7] S. S. Mirhosseini, S. Liu, J. C. Muro, Z. Liu, S. Jamali, and M. Popov, "Modeling a Voltage Source Converter Assisted Resonant Current DC Breaker for Real Time Studies," *International Journal of Electrical Power & Energy Systems*, vol. 117, p. 105678, 2020.

[8] S. Liu, A. Shetgaonkar, and M. Popov, "Coordinative Performance of HVDC Circuit Breakers in MTDC Grids," in *2020 IEEE Power & Energy Society General Meeting (PESGM)*. IEEE, 2020, pp. 1–5.

[9] S. Liu, M. Popov, S. S. Mirhosseini, S. Nee, T. Modeer, L. Ängquist, N. Belda, K. Koreman, and M. A. M. M. van der Meijden, "Modeling, Experimental Validation, and Application of VARC HVDC Circuit Breakers," *IEEE Transactions on Power Delivery*, vol. 35, no. 3, pp. 1515–1526, 2020.

[10] A. Shetgaonkar, S. Liu, and M. Popov, "Comparative Analysis of a Detailed and an Average VARC DCCB model in MTDC Systems," in *2022 IEEE Power & Energy Society General Meeting (PESGM)*, 2022, pp. 1–5.

[11] P. Wang, X.-P. Zhang, P. F. Coventry, and R. Zhang, "Start-up Control of an Offshore Integrated MMC Multi-Terminal HVDC System with reduced DC Voltage," *IEEE Transactions on Power Systems*, vol. 31, no. 4, pp. 2740–2751, 2015.

[12] L. Cai, U. Karaagac, and J. Mahseredjian, "Simulation of Startup Sequence of an Offshore Wind Farm with MMC-HVDC Grid Connection," *IEEE Transactions on Power Delivery*, vol. 32, no. 2, pp. 638–646, 2017.

[13] X. Li, C. Liu, and Y. Lou, "Start-up and recovery method with LCC-HVDC systems participation during ac/dc system black-starts," *IET Generation, Transmission & Distribution*, vol. 14, no. 3, pp. 362–367, 2020.

[14] F. Deng, Q. Heng, C. Liu, Y. Lyu, Q. Wang, D. Liu, and R. Zhu, "Circulating Current Suppression for MMC-HVDC Systems with Asymmetric Arm Impedance," *CSEE Journal of Power and Energy Systems*, vol. 7, no. 3, pp. 530–540, 2020.

[15] J. Wang, J. Liang, C. Wang, and D. Xiaoming, "Circulating Current Suppression for MMC-HVDC under Unbalanced Grid Conditions," *IEEE Transactions on Industry Applications*, vol. 53, no. 4, pp. 1–1, 03 2017.

[16] A. Shetgaonkar, A. Lekić, J. L. Rueda Torres, and P. Palensky, "Microsecond Enhanced Indirect Model Predictive Control for Dynamic Power Management in MMC Units," *Energies*, vol. 14, no. 11, 2021.

[17] H. Zhang, H. R. Wickramasinghe, L. Jing, J. Li, J. Pou, and G. Konstantinou, "Circulating Current Control scheme of Modular Multilevel Converters supplying passive networks under Unbalanced Load conditions," *Electric Power Systems Research*, vol. 171, pp. 36–46, 2019.

[18] M. Zhang, Y. Shen, H. Sun, and R. Guo, "MMC-HVDC CirculatingCurrent Suppression method based on improvedProportional Resonance control," *Energy Reports*, vol. 6, pp. 863–871, 2020.

[19] W. B4.72, "DC Grid Benchmark Models for System Studies," Brochure, 2020.

[20] A. Shetgaonkar, L. Liu, A. Lekić, M. Popov, and P. Palensky, "Model Predictive Control and Protection of MMC-based MTDC Power Systems," *International Journal of Electrical Power & Energy Systems*, vol. 146, p. 108710, 2023.

[21] Y. Huang, Y. Ji, Y. Lu, and W. Huang, "Research on Startup Circuit Parameter Selection and Startup Control Strategy for Multi-Terminal VSC HVDC System," pp. 1–7, 2019.

[22] ENTSO-E, "HVDC Links in System Operators," Technical Paper, 2019.

978-1-6654-6441-3/23/$31.00 ©2023 IEEE